Published in final edited form as:
Neuroimage. 2007 ; 37(Suppl 1): S37–S46.

Role of Neuronal Activity and Kinesin on Tract Tracing by Manganese-Enhanced MRI (MEMRI)

Elaine L. Bearer[1,3], **Tomás Luis Falzone**[2], **XiaoWei Zhang**[3], **Octavian Biris**[1], **Arkady Rasin**[1], and **Russell E. Jacobs**[3]

1 *Department of Pathology and Laboratory Medicine, Brown University, Providence, RI, 02906*

2 *Cellular and Molecular Medicine Department, Howard Hughes Medical Institute, University of California, San Diego, CA 92093-0683.*

3 *Biological Imaging Center, Beckman Institute, California Institute of Technology, Pasadena, CA 91125*

Abstract

MEMRI offers the exciting possibility of tracing neuronal circuits in living animals by MRI. Here we use the power of mouse genetics and the simplicity of the visual system to test rigorously the parameters affecting Mn^{2+} uptake, transport and trans-synaptic tracing. By measuring electrical response to light before and after injection of Mn^{2+} into the eye, we determine the dose of Mn^{2+} with the least toxicity that can still be imaged by MR at 11.7T. Using mice with genetic retinal blindness, we discover that electrical activity is not necessary for uptake and transport of Mn^{2+} in the optic nerve but is required for trans-synaptic transmission of this tracer to distal neurons in this pathway. Finally, using a kinesin light chain 1 knock-out mouse, we find that conventional kinesin is a participant but not essential to neuronal transport of Mn^{2+} in the optic tract. This work provides a molecular and physiological framework for interpreting data acquired by MEMRI of circuitry in the brain.

Keywords

MEMRI; optic track; transport; synaptic transmission; rd mutation; kinesin light chain

Introduction

Manganese-enhanced MRI (MEMRI) allows tracing of neuronal tracts in living animals, and thus offers the potential to image changes in circuitry by sequential imaging over time during evolution of disease or following exposures to experiences or drugs(Lin and Koretsky, 1997; Pautler et al., 2003). A dependence of Mn^{2+} uptake on neuronal electrical activity raises the possibility of tracing the anatomy of functional circuits. These are very exciting experimental possibilities that require rigorous testing for reliable interpretation.

Track tracing of neuronal circuits relies on a normal neuronal activity: intracellular transport. Typically tracers injected into the brain enter neurons locally and are picked up by the intracellular transport machinery and then carried along neuronal processes to reach distant

Corresponding author: Elaine L. Bearer, MD-PhD Laboratories of Molecular Medicine 70 Ship St. G-E527 Brown University Medical School Providence, RI 02903 Telephone: 401 - 863 - 3124 Fax: 401 - 863 - 9008 Email: Elaine_Bearer@Brown.edu.

synapses or cell bodies(Fritzsch, 1993; Grafstein and Forman, 1980; Lanciego et al., 2000). Transport from the synapse back to the cell body is termed “retrograde,” and from the cell body towards the synapse “anterograde”. Fast axonal transport occurs in both directions and is powered by molecular motors specific for each direction: anterograde is mediated by kinesins and retrograde by dynein and a subset of retrograde kinesins (Chevalier-Larsen and Holzbaur, 2006; Muresan, 2000; Shea and Flanagan, 2001).

The optic tract serves as an excellent test bed for monitoring transport because of its large size (~1mm in diameter) and because the majority of the axons within it are oriented in the same direction-- arising from retinal ganglion cells in the eye and projecting towards the lateral geniculate nuclei and the superior colliculus in the midbrain. Thus movement of tracers towards the brain in the optic nerve can be assumed to occur in the anterograde direction, i.e. out from the cell body, and movement towards the eye in the retrograde direction. Injection of radioactive tracers into the posterior chamber of the eye demonstrates rapid anterograde transit (2mm/hr) from the eye along the optic nerve towards the brain(Grafstein and Forman, 1980). Replicating these experiments by intravitreous injection of Mn^{2+} followed by MR imaging demonstrated that Mn^{2+} is also transported, possibly at the same rate (Pautler et al., 1998), along the optic nerve and crosses synapses to reach the visual cortex(Pautler, 1999; Pautler et al., 1998; Thuen et al., 2005; Watanabe et al., 2001; Watanabe et al., 2004).

Here, we use the power of mouse genetics to determine whether neuronal activity is required for Mn^{2+} transport and/or trans-synaptic tracing. We first test the effect of injecting Mn^{2+} into the eye on neuronal activity in the visual system. We then determine the maximum amount of Mn^{2+} that can be used to trace pathways without long-lasting damage to vision, as assessed by both physiological and morphological criteria. Next, we test whether Mn^{2+} transport is dependent on electrical activity by tracing this pathway in a blind mouse, the inbred CBA strain, lacking active photoreceptors(Caley et al., 1972). This mouse carries the *rd* mutation and has no rod light detector cells in the retina(Bowes et al., 1990). Retinal ganglion cells are intact and give rise to a robust optic nerve, but due to the absence of photoreceptor cells there is no electrical activity in the visual system in response to light. Capturing T1 weighted microMRI images at 6-minute intervals in an 11.7T MR system allowed detailed observation of transport dynamics in these various genotypes at short time intervals. Thus, minor differences in transport properties could be detected. Finally, using mice lacking the kinesin light chain 1 gene, KLC1−/− (Rahman et al., 1999), we test whether anterograde transport of Mn^{2+} is dependent on the hetero-tetrameric conventional kinesin motor coupled to this light chain. In each case, mutant mice were compared to parental strains or genetically normal littermates subjected to the same experimental protocol. Our data show that electrical activity is not required for uptake and transport of Mn^{2+} but is required for trans-synaptic transmission, and that conventional kinesin is not the only motor involved in Mn^{2+} transport.

Materials and Methods

Mouse genotypes

CBA/J mice and littermate controls at 6-12 weeks of age were obtained from Jackson Labs (Bar Harbor, ME). Sighted C57LB/6 and blind CBA (rd1−/− with retinal blindness) were analyzed for the rd1 mutation, which causes retinal blindness due to loss of photoreceptor cells. CBA/J strain carries a proviral insert in the first exon of the *Pdeb* gene, encoding the B-subunit of cGMP phosphodiesterase. Genotypes were confirmed using PCR across the transposable element insert using three primers (Table 1) as described (Gimenez and Montoliu, 2001) except for a slight correction in the RD6 primer sequence to match the accession, L02110, nucleotides 2539-2512. C57/b6 strain were used for comparison with CBA. Ten CBA mice were imaged, 5 young (6-8 weeks old) and 5 older (7-8 months old).

Kinesin light chain 1 deficient mice were previously generated by homologous recombination in a mixed 129/C57BL/6J background (Rahman 1999). Mutant mice were backcrossed into a pure C57BL/6J background for more than 12 generations. G12 male and female's heterozygote mice for KLC1 deletion were crossed against each other to obtain wild type and homozygotes mutant littermates that were used in the experiments. Mice genotyping was performed by PCR amplification of wild type and recombinant KLC1 alleles using DNA extracted from tails (Rahman 1999). Twenty-two KLC mice were examined in this study, 8 KLC−/− and 12 KLC +/+ and 2 KLC+/−. Results were highly consistent, and examples were selected to represent the average pattern to show here.

Visual Evoked potentials

Visual evoked potentials were measured before, and at 3 and 24 hours after injection of Mn^{++} into the eye using a strobe light and Labview software as described(Martin et al., 2006). Mice were anesthetized with vaporized isofluorane (1% in oxygen) and placed in a dark box kept at 37°C with a water heating pad. Three electrodes were placed, one just dorsal to the interorbital line (for measurement), the second at the nuchal crest (for reference), and the third on a rear leg (as ground). Labview software was used to collect 250 data points at a sample rate of 1 kHz recording electrical activity in response to each flash of light from a strobe light with a flash frequency of 2 Hz. Flash and measurement collection were synchronized by an external source. Data from 5 repeats of 100 flash/response measurements were averaged for each mouse at each session. VEPs were collected before Mn^{2+} injection, at 4 hr and 24 hr after Mn^{2+} injection. Input from both eyes open, one or the other eye closed, and both eyes closed were measured.

Morphological examination—Mice were anesthetized 4 months after the last MRI and sacrificed by ex-sanguination via intracardiac perfusion with a 30ml washout with warm heparinized phosphate buffered saline (PBS) followed by 50 ml of 2% paraformaldehyde (PFA) and 2.5% gluteraldehyde in 0.06 M phosphate buffer pH 7.2 at a rate of 5 ml/min. The carcass was decapitated and the head rocked in 4% PFA in PBS overnight at 4°C. All procedures were according to protocols approved by the University Committee on Animal Resources. Retina and optic tracks were dissected, diameters measured in a steroscope, and then 1mm blocks stained in aqueous 4% OsO4 at 4°C, 1% tannic acid in 0.05M Na-Cacodylate pH 7.0, followed by 0.5% Uranyl acetate in veronal acetate at 37°C, dehydrated and embedded in Epon 812. Semi-thin sections stained with toluidine blue were examined histologically for numbers and size of axons with a Zeiss axioscope and images captured with the Axiocam. Axons were counted in 4,500 μm^2 selected at random on printouts of histologic images captured at 63x magnification. Approximately 1000 axons were counted per optic tract and the average number calculated with Kaleidograph.

Magnetic resonance imaging—$MnCl_2$ (200 mM) was injected into the vitreous of the right eye. A fine steel needle (30 gauge, 0.3mm) was used to bore a hole in the sclera through which the Mn^{2+} solution was injected via a pulled glass micropipette (~10 μm tip size). The volume of injectate was monitored by calibrating the micropipette and controlling injection with a pressurized controlled picospritzer (Parker Hannifin, Cleveland, OH). MR images were acquired with an 11.7T 89 mm vertical bore Bruker BioSpin Advance DRX500 scanner(Bruker BioSpin Inc, Billerica, MA) using a 20mm RF birdcage coil. Slab images of the optic tract (0.45cm thick slab with 32 axial slices) were acquired at 6 minute intervals for 2 hours beginning 30 minutes post injection with a 3D RARE sequence (TR/TE 300/5 ms, 4 echoes, 1 averages, FOV 1.5^2×0.45 cm, and 128^2×32 matrix size for a voxel size of 140×110× 140 μm). Whole brain images were acquired at 24 h after $MnCl_2$ injection with a T_1 weighted 3D UFLARE sequence (TR/TE 300/5 ms, 4 echoes, 2 averages, FOV 2.2×1.5^2 cm, and 256×128^2 matrix size). Fro 24 hr images, standard tubes of water and of a known concentration

of gadolinium in solution and were taped to the mouse head to provide a standard for normalization of intensity values. MR images were visualized in ImageJ software and intensity normalized by setting all images to the same gray scale of the standards. In some instances, two axial slices were averaged to encompass the optic nerve as it is not straight and sometime passed out of a single slice.

ROI analysis—For analysis of dynamic imaging series, MR images from the 6 min captures were transported to ImageJ directly from the Bruker raw data. For each stack, the three slices passing through the optic track were average using Image>Stacks>Z-project. An ROI of 9 voxels was place over the optic track 1 cm from the back of the eye in the 3-slice averaged image captured at the later time point in the dynamic series when the optic track was most easily visible. The intensity was then measured in this ROI in each image in the series, beginning at the last and moving through the stack to the first without moving the ROI. Intensity in the cheek muscle was measured in parallel in each image. Average voxel intensity for each ROI in the optic track was divided by average intensity in the cheek muscle. Standard deviations in each measurement were averaged and the sum used as error bars. Unpaired student t-test was used to determine statistical significance between intensity in the wild type KLC+/+ versus in the KLC−/− in the dynamic series. For analysis of transport in the LGN and superior colliculus, similar ImageJ approach was used. The coronal slice with the most intense signal in the expected midbrain region was selected for each structure from the whole brain 24 hr 3D T1-weighted image in coronal slices. Again, average voxel intensity was acquired through an ROI of 9 voxels with ImageJ on single slices. A ROI of 26 voxels was selected in the same slice in the cheek muscle to normalize intensity measurements across scans. Intensity in the midbrain regions were divided by intensity in the standard tube. Average standard deviations were summed.

Results and Discussion

The minimal dose of $MnCl_2$ that produced reversible toxicity and MR signal

Previous tracing with MEMRI in the visual system has typically used volumes of 1-3 μl and $MnCl_2$ concentrations up to 1.0 M for injection into either the anterior chamber of the mouse eye (Lindsey et al., 2007) or the posterior chamber of the rat eye(Thuen et al., 2005). We noted that the eyes of animals so injected turned gray, and physical exam suggested that they could no longer see. We thus set out to measure visual light response as a means to determine functional effects of the injection of $MnCl_2$ on the retinal neurons and the visual system.

Light is detected in the retina by photoreceptors, which transmit signals to retinal ganglion cells that then send electrical potentials along the optic tract to the visual cortex. The electrical potential evoked by light can be measured over the visual cortex of the brain with externally placed electrodes and provides a measure of whether the visual pathway is intact. Thus, visual evoked potentials (VEP) measured before and after $MnCl_2$ injection into the eye can reveal the effect of Mn^{2+} on electrical activity in response to light in the visual pathway (Fig. 1).

Before injection, the VEP of C57 (wild type) mice was robust (Fig. 1A, top). Four hours after injection of 0.5 μl of 200 mM $MnCl_2$ into the right eye, no response to light was detected even with both eyes open. Even at 24 hr after injection, only a small late potential change was detected. Thus injection in one eye affects visual responses in the entire visual track, possibly due to cation-induced hyperpolarization in the injected eye that propagates to the visual cortex rendering it unresponsive to input from either eye.

This toxicity could be either due to $MnCl_2$ or to an increase in intraocular pressure caused by the volume of injectate. We tested a volume effect by injecting a similar amount of saline. A similar volume of saline (0.5 μl) also depressed VEPs at 4 hr after injection, but complete

recovery was evident at 24 hr (Fig. 1B). Hence, at this volume and concentration of $MnCl_2$ there was a volumetric effect.

Smaller volumes of $MnCl_2$, 0.25 μl, still depressed the light response at 4 hr but some return of function was apparent at 24 hr (Fig. 1C). Even a smaller volume, 0.125 μl and lower concentration of $MnCl_2$ (50 mM) still depressed the VEP response at 4 hr but allowed full recovery at 24 hr (Fig. 1D). Injections of 0.25 μl of saline did not cause VEP depression (Fig. 2A). Thus, 0.25 μl has no volumetric effect, and the VEP depression with this volume of $MnCl_2$ is due to the ionic composition and not the volume. Unfortunately, we could not detect optic track enhancement with a lower dose of Mn^{2+}, 0.125 μl at 50 mM. (data not shown). Thus, even doses of Mn^{2+} lower than can be detected by our 11.7T MR system depress VEPs at 4 hr after injection into the vitreous. It may be possible to detect MR signal from a lower Mn^{2+} dose with a 7T field strength. Injection into the anterior chamber could also mitigate toxicity.

Since visual response recovered at 24 hr after 0.25 μl injection of 200 mM $MnCl_2$, and since this dose produced a contrast signal detectible by MRI in the optic pathway, we opted for a 0.25 μl injection of 200 mM $MnCl_2$ for all subsequent experiments described here.

CBA mice had no response to light in the visual system

Preinjection VEPs detected no response to light in the visual system in 4-6 week old CBA mice positive for the *rd* mutation by PCR (Fig. 2B). Similar lack of response was measured in older CBA (7-14 months old). Thus, these mice are functionally blind with no detectible electrical signals in the visual pathway by VEP.

Time-lapse MR imaging of Mn^{2+} transport in the optic nerve revealed no obvious difference between blind and sighted mice

To image Mn^{2+} during transport into the optic nerve immediately after injection into the eye, we developed a pulse sequence to capture a 32-slice slab image every 6 minutes, beginning 30 min and continuing for 2 hr to conclude at 2.5 hr after injection (Fig. 3). In both C57 sighted and CBA blind mice, either young (4-6 weeks) or old (10 month), Mn^{2+}-induced signal enhancement appeared along the optic nerve over the first 2.5 hr with bright delineation of the optic tract at 24 hr.

At 30 minutes after injection MR images displayed hyper-intense signal in the vitreous of the eye that gradually decreased with time as intensity increased along the optic nerve (Fig. 3). At 30 min, signal was present in the optic nerve emerging from the eye. Over the next 2 hr, signal along the optic tract gradually increased, with no defined wave front. The rate of increase in Mn^{2+}-induced signal enhancement along the optic nerve is dependent on uptake into the ganglion cells in the retina, accumulation inside the cell, and transport along their axons. Signal enhancement was detectible at the chiasm, ~1.2 cm from the eye, at 2.5 hr suggesting a minimal transport rate of 5 mm/hr consistent with fast anterograde transport of organelles in the optic system (Brady et al., 1982;Lavail et al., 2005;Martin et al., 1999;Satpute-Krishnan et al., 2003;Shah and Cleveland, 2002).

The rate of appearance of Mn^{2+} signal along the optic nerve appeared similar in sighted and blind mice at all ages studied. This similarity demonstrates that uptake and transport are independent of electrical activity in the eye and along the optic nerve. Thus while Mn^{2+}can enter through voltage-dependent calcium channels(Merritt et al., 1989), it may also enter neurons through other ion channels, such as divalent metal transporters(Thompson et al., 2007). Once inside the cell, Mn^{2+} must complex with other molecules or enter subcellular compartment(s) for fast transport. Different compartments are known to travel at different rates

in the axon(Brady et al., 1982; Grafstein and Forman, 1980; Satpute-Krishnan et al., 2006; Thompson et al., 2007; Vale et al., 1985). For example mitochondria travel slowly (0.05-0.3 μm/sec)(Satpute-Krishnan et al., 2003) while transport vesicles in neurons may travel as fast as 5 μm/sec (Vale et al., 1985). Mn^{2+} may enter more than one of these compartments, and thus travel at various rates in the same axon.

Fewer axons are found in the optic nerve of injected eyes

Optic nerves from CBA and C57 mice fixed by perfusion several months after eye injections were examined by histology (Fig. 4) and electron microscopy (Fig. 5). By both whole mounts and in histology, the diameter of the optic nerve on the Mn^{2+} injected side was 6% less than the un-injected side (Fig. 4A, uninjected C57, Fig. 4C, injected C57, and Fig. 4D, injected CBA). This was true in either the blind CBA or the sighted C57 mouse. Histologic examination at higher magnification (Fig. 4B, E and F) suggested that in addition to decreased optic nerve diameter, there was a loss of axons and a replacement by glial or other repair tissue. Counts of axon numbers at higher magnification of histologic sections revealed 391 +/− 17 axons per 4.5 $\times 10^3$ μm^2 in the optic track of the un-injected (left) side of a C57 sighted mouse (Fig. 4B), and similar numbers in un-injected CBA mice. After injection, both CBA and C57 mice displayed fewer axons per cross sectional area of the optic nerve, with only 291 +/−4.6 axons per 4.5 $\times 10^3$ μm^2 in the optic nerve of C57 mice and 281 +/− 4.7 axons in CBA. Thus injection into the eye results in ~25% decrease in the number of axons per unit area in either blind or sighted mice. No inflammation or infection was observed in any of the histologic sections. Saline injected axons were not examined, as similar volumes produced no VEP defect and thus no axonopathy is expected.

By electron microscopy (Fig. 5) axons in the optic nerve of injected eyes from either C57-sighted or CBA-blind mice were comparable, with similar myelination and equivalent presence of neurofilaments, microtubules and mitochondria. CBA axons appeared normal in all morphological respects despite the lack of electrical stimulation from photoreceptors. Thus ultrastructural analysis of surviving axons revealed no evidence of on-going toxic effects at this time point after injection.

Transport is slowed but not abolished in KLC1−/− mice

Neuronally enriched KLC1 is one of three light chains that alternatively bind to conventional kinesin heavy chain, Kif5, to form the heterotetrameric kinesin motor(Johnson et al., 1990; Lamerdin et al., 1996; Rahman et al., 1998; Rahman et al., 1999).

To test whether this form of kinesin was involved in Mn^{2+} transport, we used KLC1 knockout mice that lack this type of light chain(Rahman et al., 1999; Vale et al., 1985). These mice have alterations in kinesin behavior. At 24 hr after injection into the right eye, enhancement of the optic tract in KLC1 knockouts was similar to littermates. However at earlier time points Mn^{2+} enhancement developed more slowly (Fig. 6). At 2.5 hr after injection, the optic track remained difficult to identify in KLC1 −/− mice, even though in all other mice assessed enhancement was obvious by this time point. Because accumulation of signal is gradual, this difference might not have been detected had we only captured 24 hr images.

Since Mn^{2+} enters cells and associates either with protein complexes or membranes, it may associate with a subset of cargo complexes that depend on KLC1 for their transport(Bowman et al., 2000; Kamal et al., 2000; Verhey et al., 2001). The lack of KLC1 in mutants would thus produce a decrease in the number and/or speed of Mn^{2+}-containing vesicles being transported and thus a delay in the early wave of Mn^{2+} transport towards the chiasm, as observed here in the time-lapse sequence. By 24 hr this slower accumulation was sufficient to produce signal along the optic tract similar to C57/b6 and to littermates with KLC1+/+ genotype. Hence

similarity at later time points to wildtype may be explained by the transport of Mn^{2+} in KLC1 −/− being mediated by motors other than conventional kinesin with the KLC1 light chain.

ROI analysis of the intensity changes in the optic track during the first 2.5 hr after injection demonstrate that in KLC+/+ intensity increased at 1 cm from the eye by 150% while in KLC −/− no increase is detected (Fig. 6C). Unpaired students t-test demonstrated that this difference in intensity has a probability of 0.0001 of occurring by chance.

Repair is depressed in KLC1 knockout mice

VEP analysis of KLC1 knockouts revealed a defect in restoration of the normal light response at 24 hr after Mn^{2+} injection (Fig. 7). In normal littermates, VEPs at 24 hr were analogous to pre-injection depolarizations after right eye injection, with only a slight delay in response and minor alterations in voltage restitution after depolarization (Fig. 7A). In KLC knockouts, at 24 hr after Mn^{2+} injection into the right eye, voltage change in response to light was both delayed and depressed (Fig. 7B). Thus, these KLC1 −/− animals do not repair the visual system as completely as the other genotypes surveyed here, which could also be a consequence of decreased transport.

Trans-synaptic tracing by Mn^{2+} requires neuronal activity

Previous studies have demonstrated that Mn^{2+} signal crosses synapses and thus traces circuits beyond those of single neuronal projections(Murayama et al., 2006; Pautler et al., 2003; Saleem et al., 2002). To determine whether this trans-synaptic transmission was dependent on neuronal activity, studies have relied on experiential stimulation of the particular pathway involved. However, to apply Mn^{2+} tract tracing to unknown pathways, it will be important to know definitively whether trans-synaptic transmission requires neuronal activity. The blind mice used in this study provide a more rigorous test for this analysis.

Mn^{2+} injection into the eye results in tracing of the visual system across at least two synapses: first, retinal ganglion cell projections onto the midbrain, and second, midbrain neurons onto the visual cortex(Lindsey et al., 2007; Murayama et al., 2006; Pautler et al., 1998; Thuen et al., 2005; Watanabe et al., 2001). The amount of transfer across synapses appears to correlate with axonal caliber (Murayama et al., 2006).

Three dimensional whole brain images of mouse brains 24 hr after Mn^{2+} injection into the eye resulted in Mn^{2+}-induced enhancement in the midbrain of KLC1+/+ wildtype, and KLC−/− mice, despite the initial slower transport in the knockouts (Fig. 8). However, in blind mice lacking neuronal activity in the visual system, little Mn^{2+} signal was detected in either the lateral geniculate nucleus or the superior colliculus in the midbrain. This is despite robust signal along the optic track and an equivalent number and caliber of axons as determined by our histological examination reported earlier in this paper (Fig. 4-5).

ROI analysis of the intensity in the eye, optic track and midbrain in the three types of mice examined here (wildtype, KLC−/− and CBA) at 24 hr after eye injection (Fig. 8B) demonstrated (1) similar intensity in all three mice in the eye, (2) slight (20%) decrease intensity in the optic tract in KLC−/− and CBA compared to wildtype, (3) significantly less intensity (80-90% less) in midbrain trans-synaptic sites in blind (CBA) compared to wildtype and KLC−/− mice.

Thus, while Mn^{2+} uptake and transport within the neuron occur independent of electrical activity, Mn^{2+} is not transmitted efficiently across synapses in the absence of electrical activity in this system.

Conclusion

Here we show that Mn^{2+} injection into the eye disrupts the electrical response to light in the visual system. At high volumes (>0.25 μl) of injectate there is a volumetric effect. At low volumes (in mouse, <0.25 μl of 200 mM) a transient effect on VEP which reverses after 24 hr was observed with Mn^{2+} but not with saline. Even at these low amounts, a permanent loss of 10-20% of the axons in the optic nerve was found. Hence Mn^{2+} exposure may have long-term effects on neurons. Uptake and transport of Mn^{2+} in the optic nerve occurred in blind mice with no detectible electrical activity in the visual system. Thus Mn^{2+} does not require electrical activity to enter neurons and trace their individual processes. However, Mn^{2+} did not appear in the midbrain in blind mice, demonstrating that Mn^{2+} required neuronal activity to cross these synapses. Mice defective in one of the conventional kinesin light chains, KLC1, displayed slower accumulation of Mn^{2+} along the optic nerve but no decrease in trans-synaptic tracing. Therefore, Mn^{2+} is not transported by KHC-KLC1 motor alone, other motors must be involved. Thus the volume and concentration of Mn^{2+} injected for tracing must be carefully monitored, and electrical activity of neuronal pathways will affect the efficiency of tracing circuits across synapses.

Dependency on electrical activity of trans-neuronal transmission of Mn^{2+} makes this tracer particularly useful for the study of progression of neurodegenerative disease. New hypotheses in Alzheimer's disease and other neurodegenerative diseases propose that synapse loss is one of the earliest events that correlate with memory impairments. Mn^{2+} transport rates and trans-neuronal track tracing may thus be useful both to delineate anatomical projections of neurons as well as to study anatomical and functional activity within individual neurons and along circuits crossing several synapses. Mn^{2+} tracing will reveal the evolution of dysfunction in neuronal circuitry in mouse models of disease and thus may provide significant insights about disease progression not easily obtainable by any other means.

Acknowledgements

We thank Scott Fraser at Caltech and Larry Goldstein at UCSD for their support, and Tim Hiltner and Jean Edens for technical assistance. We gratefully acknowledge the Moore Foundation for awarding a Moore Distinguished Scholar to E.L.B. which funded her to work at Caltech while on sabbatical from Brown. The project was also funded in part by NIH NIGMS GM47368, NINDS NS046810 and P20 RR018757 (E.L.B.), NCRRBIRN (R.E.J.) and the Pew Fellow Program and The American Parkinson Disease Association (T.L.F).

References

Bowes C, Li T, Danciger M, Baxter LC, Applebury ML, Farber DB. Retinal degeneration in the rd mouse is caused by a defect in the beta subunit of rod cGMP-phosphodiesterase. Nature 1990;347:677–680. [PubMed: 1977087]

Bowman AB, Kamal A, Ritchings BW, Philp AV, McGrail M, Gindhart JG, Goldstein LS. Kinesin-dependent axonal transport is mediated by the sunday driver (SYD) protein. Cell 2000;103:583–594. [PubMed: 11106729]

Brady ST, Lasek RJ, Allen RD. Fast axonal transport in extruded axoplasm from squid giant axon. Science 1982;218:1129–1131. [PubMed: 6183745]

Caley DW, Johnson C, Liebelt RA. The postnatal development of the retina in the normal and rodless CBA mouse: a light and electron microscopic study. Am J Anat 1972;133:179–212. [PubMed: 5009246]

Chevalier-Larsen E, Holzbaur EL. Axonal transport and neurodegenerative disease. Biochim Biophys Acta 2006;1762:1094–1108. [PubMed: 16730956]

Fritzsch B. Fast axonal diffusion of 3000 molecular weight dextran amines. Journal of Neuroscience Methods 1993;50:95–103. [PubMed: 7506342]

Gimenez E, Montoliu L. A simple polymerase chain reaction assay for genotyping the retinal degeneration mutation (Pdeb(rd1)) in FVB/N-derived transgenic mice. Lab Anim 2001;35:153–156. [PubMed: 11315164]

Grafstein B, Forman DS. Intracellular transport in neurons. Physiological Reviews 1980;60:1168–1283.

Johnson CS, Buster D, Scholey JM. Light chains of sea urchin kinesin identified by immunoadsorption. Cell Motil Cytoskeleton 1990;16:204–213. [PubMed: 2142020]

Kamal A, Stokin GB, Yang Z, Xia CH, Goldstein LS. Axonal transport of amyloid precursor protein is mediated by direct binding to the kinesin light chain subunit of kinesin-I. Neuron 2000;28:449–459. [PubMed: 11144355]

Lamerdin JE, Stilwagen SA, Ramirez MH, Stubbs L, Carrano AV. Sequence analysis of the ERCC2 gene regions in human, mouse, and hamster reveals three linked genes. Genomics 1996;34:399–409. [PubMed: 8786141]

Lanciego JL, Wouterlood FG, Erro E, Arribas J, Gonzalo N, Urra X, Cervantes S, Gimenez-Amaya JM. Complex brain circuits studied via simultaneous and permanent detection of three transported neuroanatomical tracers in the same histological section. J Neurosci Methods 2000;103:127–135. [PubMed: 11074102]

Lavail JH, Tauscher AN, Hicks JW, Harrabi O, Melroe GT, Knipe DM. Genetic and molecular in vivo analysis of herpes simplex virus assembly in murine visual system neurons. J Virol 2005;79:11142–11150. [PubMed: 16103165]

Lin YJ, Koretsky AP. Manganese ion enhances T-1-weighted MRI during brain activation: An approach to direct imaging of brain function. MagnResonMed 1997;38:378–388.

Lindsey JD, Scadeng M, Dubowitz DJ, Crowston JG, Weinreb RN. Magnetic resonance imaging of the visual system in vivo: Transsynaptic illumination of V1 and V2 visual cortex. Neuroimage 2007;34:1619–1626. [PubMed: 17204432]

Martin M, Iyadurai SJ, Gassman A, Gindhart JG Jr. Hays TS, Saxton WM. Cytoplasmic Dynein, the Dynactin Complex, and Kinesin Are Interdependent and Essential for Fast Axonal Transport. Mol Biol Cell 1999;10:3717–3728. [PubMed: 10564267]

Martin M, Reyes SD, Hiltner TD, Givogri MI, Tyszka JM, Fisher R, Campagnoni AT, Fraser SE, Jacobs RE, Readhead C. T(2)-weighted muMRI and Evoked Potential of the Visual System Measurements During the Development of Hypomyelinated Transgenic Mice. Neurochem Res 2006;32:159–165. [PubMed: 16927171]

Merritt JE, Jacob R, Hallam TJ. Use of manganese to discriminate between calcium influx and mobilization from internal stores in stimulated human neutrophils. J Biol Chem 1989;264:1522–1527. [PubMed: 2536366]

Murayama Y, Weber B, Saleem KS, Augath M, Logothetis NK. Tracing neural circuits in vivo with Mn-enhanced MRI. Magn Reson Imaging 2006;24:349–358. [PubMed: 16677940]

Muresan V. One axon, many kinesins: What's the logic? J Neurocytol 2000;29:799–818. [PubMed: 11466472]

Pautler, R. In Vivo Neuronal Tract Tracing Utilizing Manganese Enhanced MRI (MEMRI). Carnegie Mellon University; 1999. PhD Thesis

Pautler RG, Mongeau R, Jacobs RE. In vivo trans-synaptic tract tracing from the murine striatum and amygdala utilizing manganese enhanced MRI (MEMRI). Magn Reson Med 2003;50:33–39. [PubMed: 12815676]

Pautler RG, Silva AC, Koretsky AP. In vivo neuronal tract tracing using manganese-enhanced magnetic resonance imaging. Magn Reson Med 1998;40:740–748. [PubMed: 9797158]

Rahman A, Friedman DS, Goldstein LS. Two kinesin light chain genes in mice. Identification and characterization of the encoded proteins. J Biol Chem 1998;273:15395–15403. [PubMed: 9624122]

Rahman A, Kamal A, Roberts EA, Goldstein LS. Defective kinesin heavy chain behavior in mouse kinesin light chain mutants. J Cell Biol 1999;146:1277–1288. [PubMed: 10491391]

Saleem KS, Pauls JM, Augath M, Trinath T, Prause BA, Hashikawa T, Logothetis NK. Magnetic resonance imaging of neuronal connections in the macaque monkey. Neuron 2002;34:685–700. [PubMed: 12062017]

Satpute-Krishnan P, DeGiorgis JA, Bearer EL. Fast anterograde transport of herpes simplex virus: role for the amyloid precursor protein of Alzheimer's disease. Aging Cell 2003;2:305–318. [PubMed: 14677633]

Satpute-Krishnan P, DeGiorgis JA, Conley MP, Jang M, Bearer EL. A peptide zipcode sufficient for anterograde transport within amyloid precursor protein. Proc Natl Acad Sci U S A 2006;103:16532–16537. [PubMed: 17062754]

Shah JV, Cleveland DW. Slow axonal transport: fast motors in the slow lane. Curr Opin Cell Biol 2002;14:58–62. [PubMed: 11792545]

Shea TB, Flanagan LA. Kinesin, dynein and neurofilament transport. Trends Neurosci 2001;24:644–648. [PubMed: 11672808]

Thompson K, Molina RM, Donaghey T, Schwob JE, Brain JD, Wessling-Resnick M. Olfactory uptake of manganese requires DMT1 and is enhanced by anemia. Faseb J 2007;21:223–230. [PubMed: 17116743]

Thuen M, Singstad TE, Pedersen TB, Haraldseth O, Berry M, Sandvig A, Brekken C. Manganese-enhanced MRI of the optic visual pathway and optic nerve injury in adult rats. J Magn Reson Imaging 2005;22:492–500. [PubMed: 16161073]

Vale RD, Schnapp BJ, Reese TS, Sheetz MP. Organelle, bead, and microtubule translocations promoted by soluble factors from the squid giant axon. Cell 1985;40:559–569. [PubMed: 2578887]

Verhey KJ, Meyer D, Deehan R, Blenis J, Schnapp BJ, Rapoport TA, Margolis B. Cargo of kinesin identified as JIP scaffolding proteins and associated signaling molecules. J Cell Biol 2001;152:959–970. [PubMed: 11238452]

Watanabe T, Michaelis T, Frahm J. Mapping of retinal projections in the living rat using high-resolution 3D gradient-echo MRI with Mn2+-induced contrast. Magn Reson Med 2001;46:424–429. [PubMed: 11550231]

Watanabe T, Radulovic J, Spiess J, Natt O, Boretius S, Frahm J, Michaelis T. In vivo 3D MRI staining of the mouse hippocampal system using intracerebral injection of MnCl2. Neuroimage 2004;22:860–867. [PubMed: 15193616]

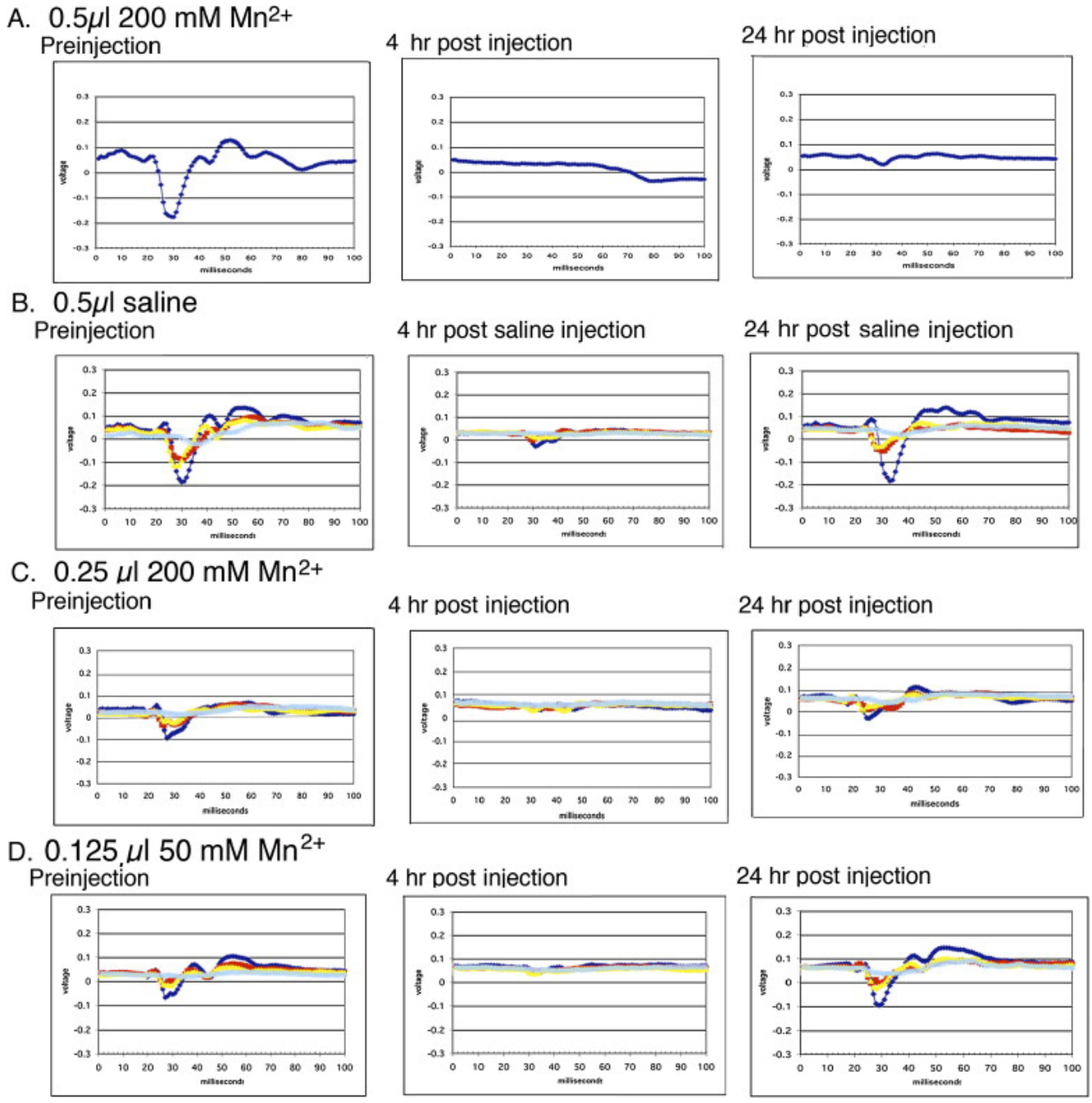

Figure 1. Mn^{2+} injection into the eye affects electrical activity in response to light

Shown are graphs of averaged VEP measurements before, 4 hr, and 24 hr after injection of various volumes of Mn^{2+} or saline solutions into the right eye of sighted C57/b6 mice (A-D). In Fig.1A, VEP was measured with both eyes open. In B-D, VEPs were measured from the injected right eye (red), the un-injected left eye (yellow), both eyes open (dark blue) or both eyes closed (light blue). Full recovery occurred at 24 hr at lower doses.

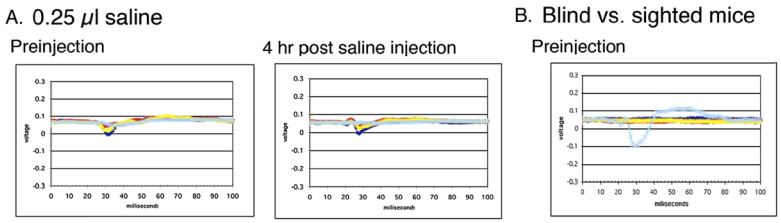

Figure 2. Injection of 0.25 μl saline has no effect on visual evoked potentials. CBA mice with rd−/− have no response to light by VEP

(A) Injection of 0.25 μl saline had no effect on VEP of C57 wildtype mice at 4 hr (color code is the same as in Fig. 1). (B) Preinjecton VEP measurements of three different CBA mice with both eyes open demonstrated that they were functionally blind (CBA: red, yellow, and dark blue) with no light response as compared to a C57 mouse tested on the same day (C57: light blue).

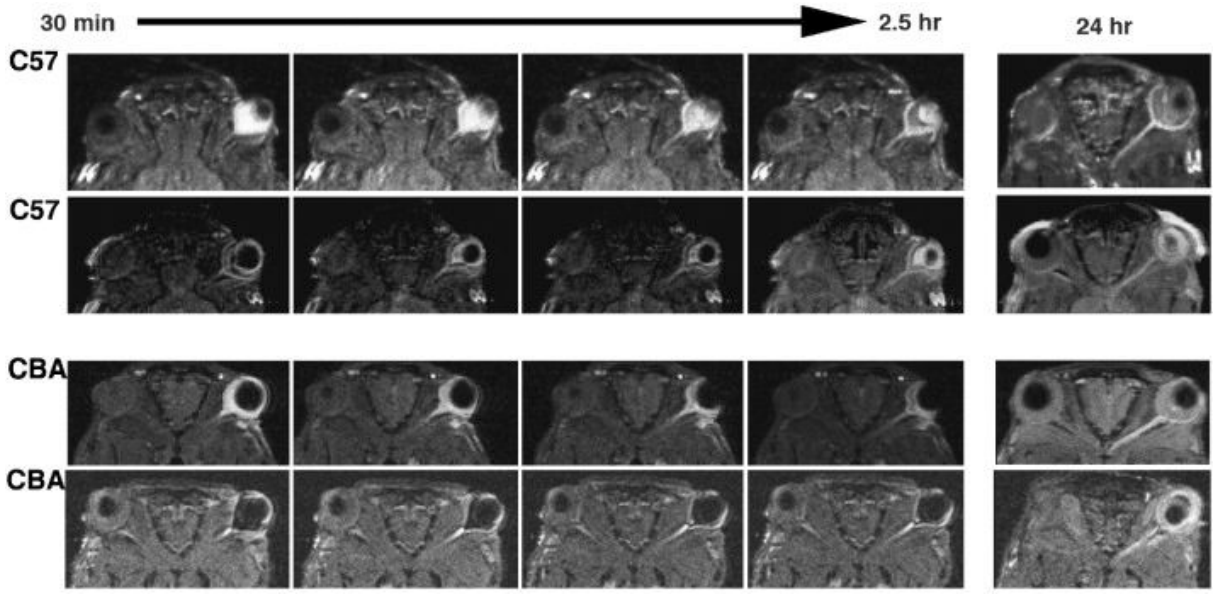

Figure 3. Time-lapse MRI of optic nerve enhancement after Mn^{2+} injection into the right eye of sighted and blind mice

Shown are representative images of four of the mice used in this study, two sighted C57 and two blind CBA. In each pair, the top sequence is from a young (6-8wk old) mouse and the lower from an older (7 mo old) mouse. Images were captured at every 6 min. Shown are images selected from these time-lapse sequences, beginning with the first, captured at 30 min post-injection, and then at 1 hr, 1.5 hr and 2.5 hr post injection. At 24 hr after injection a similar slab image bracketing the optic tract was captured. Similar images were obtained for all 5 CBA young, 5 CBA old and 7 C57 mice of any age.

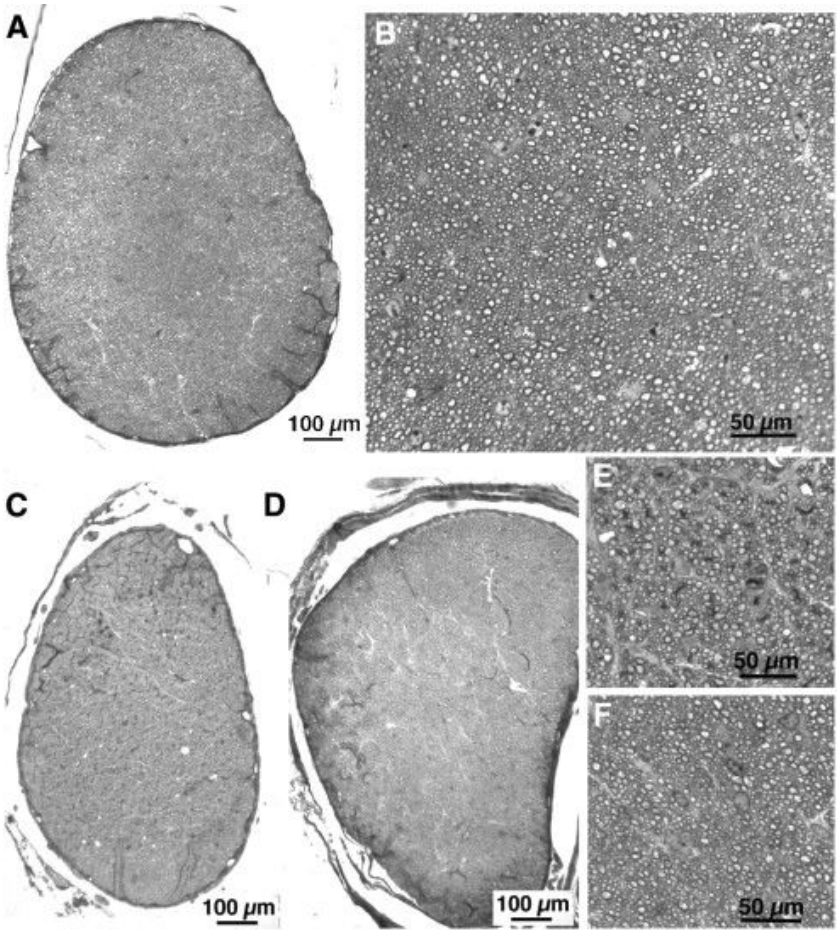

Figure 4. Long-term effects of Mn^{2+} injection by histology

Optic nerve from an uninjected C57 mouse at low magnification (A) and high magnification (B), and optic nerves from injected eye of C57 (C and E) and of CBA blind mouse (D and F).

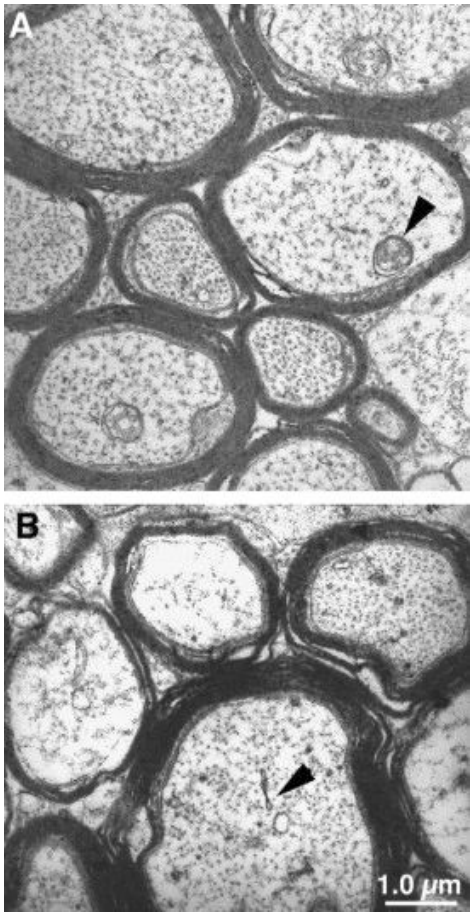

Figure 5. Ultrastructure of axons in the optic nerve from Mn^{2+} injected eyes

Representative examples of axons imaged by TEM within the right optic nerve of sighted C57 mouse (A) and blind CBA mouse (B) each injected with Mn^{2+} in the right eye are shown. Note the dark myelin sheath encircling the axons, the dots within the axons representing cytoskeletal elements in cross section, and the presence of cytoplasmic organelles within the axons (arrowheads).

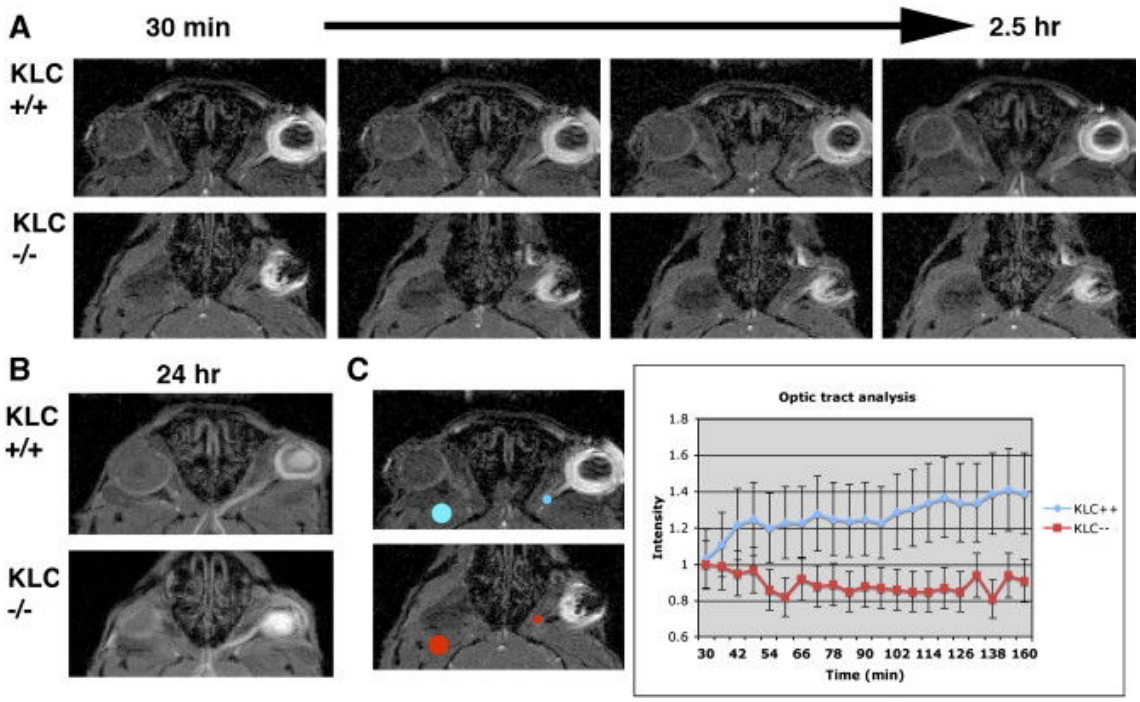

Figure 6. Time-lapse MRI of optic nerve enhancement after Mn^{2+} injection into the right eye of KLC+/+ (wildtype littermate) and KLC −/− mice

A) Representative images from two time-lapse sequences, KLC+/+ (top) and KLC −/− mice, captured at 30 min, 1, 1.5 and 2.5 hr after injection of 0.25 μl of 200 mM Mn^{2+} into the right eye. Note that by 2.5 hr after injection in the littermate, Mn^{2+} signal is present along the optic nerve possibly reaching the chiasm. In contrast in the KLC−/− mouse, Mn^{2+} enhancement is only detected in a short segment at the beginning of the optic nerve. B) At 24 hr Mn^{2+} signal has progressed along the optic track in both genotypes, demonstrating that the optic tract is intact. C) ROI intensity measurement (position indicated by circles in left panel) demonstrate that over the first 160 min after Mn^{2+} injection into the vitreous, intensity (the ratio of optic track vs. cheek muscle) increased in the optic tract by 150% in the wildtype KCL++ while no intensity increase was detected in the KLC−/− mouse. Error bars represent the sum of the standard deviations of the average voxel intensities in optic tract vs cheek muscle ROIs. For KLC+/+ these were 10% and 6 % respectively, and for KLC−/− 7% and 6%.

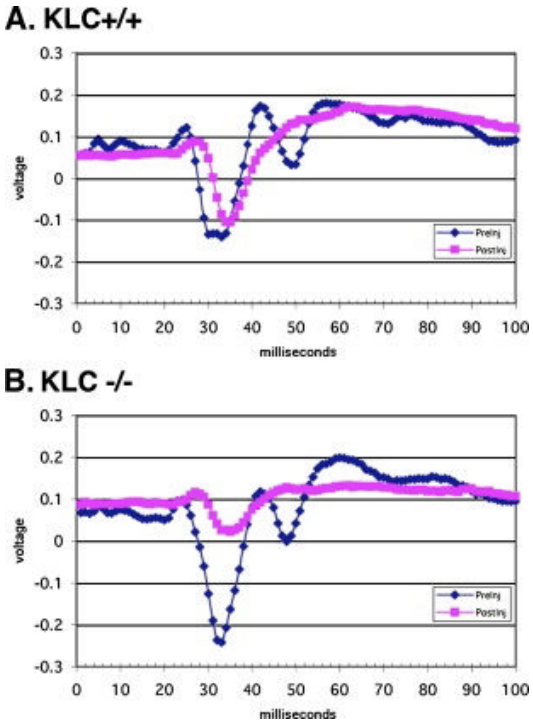

Figure 7. VEP of KLC mice

Shown are examples of VEPs from two mice, one KLC +/+ littermate (A) and one KLC −/− knockout (B) before (blue) and at 24 hr (magenta) after Mn^{2+} injection into the right eye. Note the delayed response to light after Mn^{2+} injection in both types of mouse, and the significant decrease in signal intensity in the knockout at 24 hr.

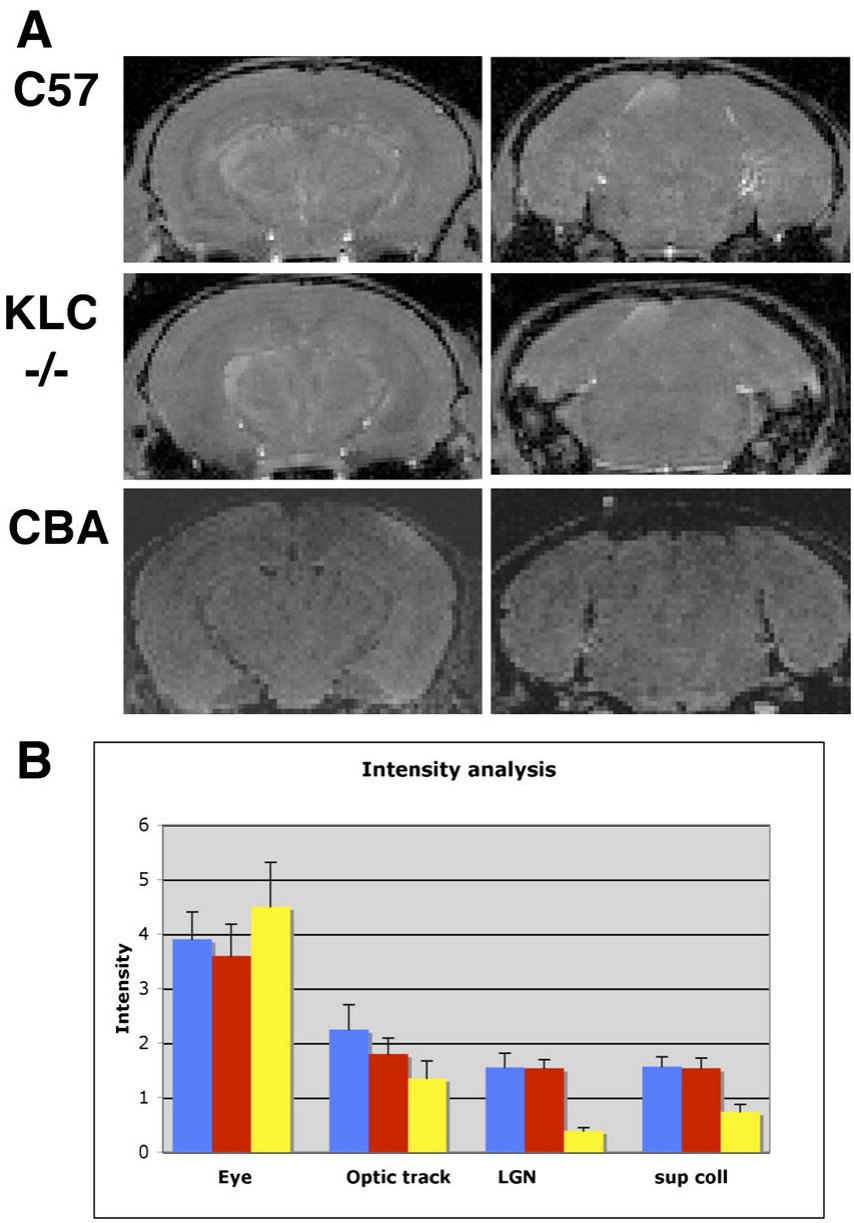

Figure 8. Mn^{2+} enhancement is greater in the midbrain at 24 hr post eye injection in C57/b6, KLC −/− knockouts, than in blind CBA mice

A) Coronal sections through the midbrain taken from 3D MR images captured at 24 hr post Mn^{2+} injection into the right eye are shown for mouse genotypes as indicated. Sections through the lateral geniculate (left panels) or the superior colliculus (right panels) demonstrate Mn^{2+} induced increased intensity in C57 and KLC1−/− but no obvious increase in the blind CBA mouse. B) ROI analysis of intensity in the eye, optic track, and midbrain (lateral geniculate nucleus (LGN); and superior colliculus (sup coll). Wildtype (KLC+/+) is shown in blue, KLC −/− in red, and rd−/− (blind) mice in yellow. Intensity values represent the ratio of average voxel intensity in optic tract vs. standard tube, Error bars represent the sum of the standard deviations of voxel intensities of the ROIs and the standard tube.

Table 1

Strategy to determine the presence of the rd−/− mutation

Retinal blindness in the CBA mouse is caused by a proviral insert into intron I of the *Pdeb* gene which interferes with normal transcription (top, diagram, adapted from Gimenez and Montoliu, 2001). The primer set that crosses this insertion site (RD6 and RD3) produces a 0.4 kb product in rd+/+ mice lacking the insert and a much larger 9.1 kb product (not detectible) in rd−/− containing the insert. The converse is true when primer RD4 within the proviral insert is combined with downstream intron primer RD3. In this case, PCR from DNA from rd−/− mouse produces a 0.55kb product but no product is produced from rd+/+. If both alleles had been present, then two products, one for each primer set, would be obtained. All mice in this study displayed only one product and thus were homozygous for either rd+/+ or rd−/−.

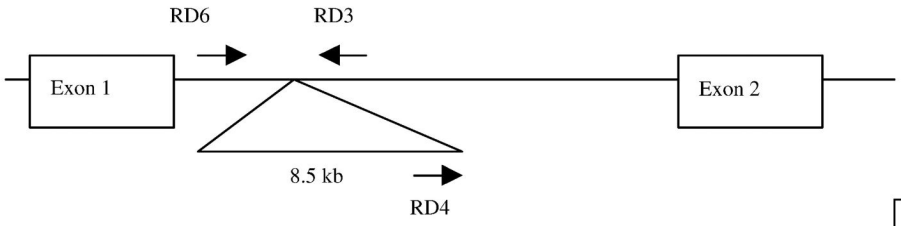

Primer name	Primer sequence
RD 3	TGACAATTACTCCTTTTCCCTCAGTCTG
RD 4	GTAAACAGCAAGAGGCTTTATTGGGAAC
RD 6	TACCCACCCTTCCTAATTTTTCTCACGC